THE ASTROPHYSICAL JOURNAL, 352:207–221, 1990 March 20

PULSAR FLUX STABILITY AND REFRACTIVE INTERSTELLAR SCINTILLATION

DANIEL R. STINEBRING
Joseph Henry Laboratories and Physics Department, Princeton University

AND

J. J. CONDON
National Radio Astronomy Observatory
Received 1988 February 24; accepted 1989 September 12

ABSTRACT

We have measured accurate flux densities of 25 pulsars at 310, 416, and 750 MHz for 43 consecutive days with the NRAO 91 m telescope. We chose pulsars covering a wide range of dispersion measures (DM) to distinguish intrinsic luminosity variations from diffractive and refractive interstellar scintillations (RISS). The pulsars PSR 1818−04, 1933+16, and 2111+46 have such high DMs and/or low space velocities that their predicted RISS time scales at low frequencies are $\gg$43 days. These pulsars were observed to have quite constant flux densities, implying that their luminosities must be intrinsically stable on time scales from several minutes (the duration of a single flux-density measurement) to several weeks (the duration of the experiment). Since the DM is primarily a property of the interstellar medium along the line of sight to a pulsar, rather than of the pulsar itself or its environment, we conclude that most pulsars have intrinsically stable luminosities. A number of pulsars with intermediate dispersion measures (e.g., PSR 0329+54) showed moderate ($\Delta S/\langle S\rangle \approx$ 0.3) flux-density variations on time scales from days to weeks. We ascribe these variations to refraction in the interstellar medium. It follows that an intrinsically nonvariable extragalactic source whose angular diameter is not much larger than the scattering angle θ should also scintillate. The observed values $\theta \approx 10^{-4}$ to 10^{-3} arcsec approach the angular sizes of the most compact extragalactic sources at these frequencies, so our pulsar observations confirm the suggestion of Rickett, Coles, and Bourgois that low-frequency ($\nu \leq 1$ GHz) variability of extragalactic sources can be caused by RISS.

Subject headings: interstellar: matter — pulsars

I. INTRODUCTION

Variability in the observed flux densities of compact radio sources can be produced by intrinsic luminosity changes or by propagation effects along the line of sight. Interstellar electron-density inhomogeneities on scales 10^9–10^{11} cm cause *diffractive* interstellar scintillations (hereafter DISS), rapid (minutes to hours) flux-density variations in pulsars (Scheuer 1968; Cordes, Weisberg, and Boriakoff 1985). Motion of the line of sight between the pulsar and Earth with respect to the interstellar medium is needed to produce the time variations; the inhomogeneities themselves are essentially "frozen in." Pulsars are the only known sources that are sufficiently compact to exhibit strong DISS. DISS fluctuations along lines of sight separated by more than $\approx 10^{-7}$ arcsec add incoherently, reducing the intensity modulation index $m_I \equiv \sigma_I/\langle I\rangle$ of an extended source, where $\sigma_I = \langle (I - \langle I\rangle)^2\rangle^{1/2}$ and the angle brackets denote a time average. At 430 MHz even the most compact ($\theta \approx 10^{-3}$ arcsec) extragalactic sources have undetectably low ($m_I < 10^{-3}$) DISS modulation indices (Dennison and Condon 1981, and references therein). Rickett, Coles, and Bourgois (1984) have pointed out that *refraction* by larger scale (10^{11}–10^{13} cm) electron-density inhomogeneities will cause focusing and defocusing of rays from a distant Galactic or extragalactic radio source. Refraction might produce slow (days to years) intensity variations, or refractive interstellar scintillations (RISS), in Galactic pulsars and possibly in compact extragalactic sources.

Long-term pulsar intensity variations were first studied by Cole, Hesse, and Page (1970) and Helfand, Fowler, and Kuhlman (1977, hereafter HFK). They found nonperiodic intensity fluctuations with a characteristic time scale of tens of days at 156 MHz and 390 MHz. Sieber (1982) pointed out that these time scales were correlated with the dispersion measures of the seven pulsars studied and concluded that the flux variations were probably caused by propagation effects in the interstellar medium, motivating the Rickett, Coles, and Bourgois (1984) hypothesis. The theory behind RISS has been developed further in a series of papers (Blandford and Narayan 1985; Goodman and Narayan 1985; Romani, Narayan, and Blandford 1986; Cordes, Pidwerbetsky, and Lovelace 1986). These authors have presented results for refraction in an extended medium and for a variety of density inhomogeneity spectra, including spectra for which large-scale inhomogeneities dominate the refraction. Other work (Cawthorne and Rickett 1985; Rickett 1986) has emphasized the potential importance of this phenomenon in explaining intensity variations of compact extragalactic sources (e.g., Altschuler *et al.* 1984), the small-amplitude "flicker" of flat-spectrum extragalactic sources (Heeschen 1984; Simonetti, Cordes, and Heeschen 1986; Blandford, Narayan, and Romani 1986), the variability of Galactic continuum sources (Taylor and Gregory 1983), and the presence of isolated scattering events that might cause dramatic intensity variations (Fiedler *et al.* 1987; Romani, Blandford, and Cordes 1987). An excellent summary of the state of RISS studies can be found in the conference proceedings edited by Cordes, Rickett, and Backer (1988).

Although RISS has received a considerable amount of theoretical attention, it is not well studied observationally. This is particularly true for pulsars, the only sources which exhibit DISS and can be used as point-source calibrators of the RISS

phenomenon. Cole, Hesse, and Page (1970) made daily observations of five pulsars at 81.5 MHz for 11 months. They found moderate modulation on a time scale of several weeks for those nearby pulsars. Hesse (1972) made daily observations of three pulsars at 81.5 MHz and 151 MHz, finding a substantial correlation in flux variations at the two frequencies. HFK studied seven pulsars at 156 MHz and 390 MHz and reported roughly equal time scales at the two frequencies and substantial intensity modulation. McAdam (1981) showed that the Vela pulsar, PSR 0833−45, underwent large intensity fluctuations during a 12 yr period. A number of careful studies of diffractive pulsar scintillation have been made in recent years (e.g., Hewish, Wolszczan, and Graham 1985; Cordes and Wolszczan 1986) that show how refractive effects introduce non-random patterns in the DISS fluctuations.

Nevertheless, there is still much that is not known about RISS. The depth of RISS intensity modulation has not been well determined, there has been no quantitative comparison between predicted and observed values of the RISS time scale T_r, and the scaling of modulation depth and time scale with frequency is not well established. All of these quantities are important for checking the validity of various theoretical assumptions and for distinguishing between different models of the interstellar medium. They are also useful for deciding whether RISS can cause the observed low-frequency variability of extragalactic sources.

In this paper we report the results of an extensive study of RISS using pulsars as point-source probes of the interstellar medium. We concentrate on three major questions: (1) Are pulsar luminosities intrinsically stable enough to be useful for quantitative studies of RISS? (2) What is the point-source modulation depth of RISS? (3) Can RISS be responsible for low-frequency variability of "extended" extragalactic sources with intrinsic angular diameters $\theta_i \approx 10^{-3}$ arcsec? We discuss our observing and analysis procedures in § II and present the results of the observations in § III. We summarize our findings in § IV.

II. OBSERVATIONS AND DATA ANALYSIS

a) Observing Procedure

We selected 25 pulsars for daily flux-density monitoring. These pulsars have $10.7 \leq DM \leq 158$ pc cm^{-3} and, for the most part, known DISS parameters. The observations are summarized in Table 1. For each pulsar we list the observing frequency ν, the dispersion measure DM, the number of days over which the observations extended N (the /2 notation indicates sampling every other day), the average number of pulses in an observation $\langle M \rangle$, and the mean continuum flux density observed $\langle S \rangle$. The seventh and eighth columns are values of the DISS decorrelation bandwidth $\Delta\nu_d$ and the decorrelation time scale T_d taken from Cordes, Weisberg, and Boriakoff (1985) and scaled to the observing frequency using equations (A9) and (A10) assuming $\alpha = 11/3$, the Kolmogorov value. The ninth column is the transverse velocity of the pulsar, derived from DISS parameters by Cordes (1986). The tenth column lists the predicted RISS time scale T_r, calculated using equation (A12).

Our observations were made during the interval 1984 August 16–September 28 with the NRAO[1] 91 m transit telescope in Green Bank, West Virginia. A daily pulsar observation normally consisted of separate flux-density measurements made at 310 MHz, 416 MHz, and 750 MHz while the pulsar was being tracked continuously with the low-frequency traveling feed system. The total integration time at each frequency was about 5 minutes. During each flux-density measurement the Nicolet signal averager accumulated separate 2048 point pulse-synchronous averages of the detected outputs in two orthogonal linear polarizations. Both averages were written onto magnetic tape every 10 s. The results of a typical pulsar observation are shown in Figure 1. Since the maximum tracking time per source with the traveling feed is only about 25 sec δ minutes, some pulsars in crowded right ascension ranges were observed at only one or two frequencies or were observed every other day rather than daily. Otherwise, the observations were identical on the 43 consecutive days of our observing run.

In order to minimize interference, we used observing bandwidths of 3 MHz at the two lower frequencies and 10 MHz at the higher frequency. Dispersion smearing across these bandwidths is generally much smaller than either the postdetection time constant (3 ms) or the pulse width, except for a few short-period, high–DM pulsars. In these cases, dispersion smearing broadened the pulses but had no effect on the time-averaged flux densities measured, aside from lowering the signal-to-noise ratios of the observations. In most cases receiver noise was not the limiting factor in our flux-density measurements. Our observing bandwidths were not significantly larger than the DISS decorrelation bandwidths ν_d of pulsars with the lowest

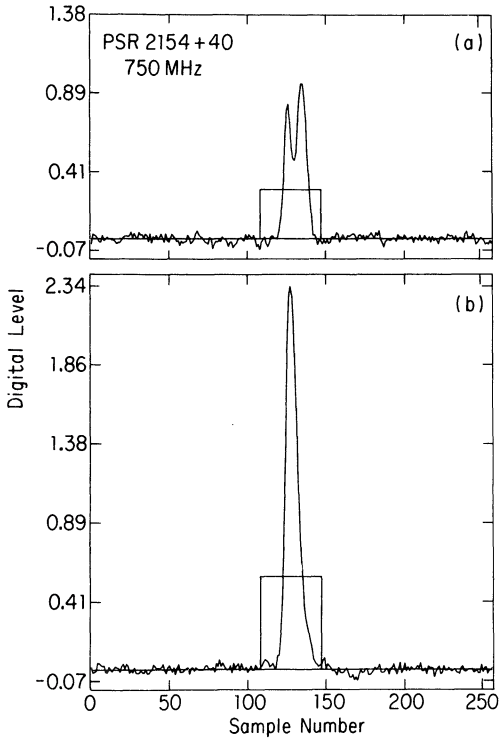

FIG. 1.—Results from a single 5 minute scan of PSR 2154+40 at 750 MHz. Separate profiles were obtained for orthogonal linear polarizations (*a*) and (*b*). The original 2048 point profiles were smoothed to 256 points and phase-shifted to center the pulse before linear baselines were subtracted. The area under each rectangle is equal to the area under the pulse. The abscissa is the sample number; the ordinate is the uncalibrated flux density (digital levels).

[1] The National Radio Astronomy Observatory is operated by Associated Universities, Inc., under contract with the National Science Foundation.

TABLE 1

OBSERVATIONAL SUMMARY

PSR	ν (MHz)	DM (pc cm^{-3})	N	<M>	<S> (mJy)	log $\Delta\nu_d$ (MHz)	T_d (s)	$v_\perp$ (km s^{-1})	T_r (days)
0031–07	310	10.9	39	656	159	–0.60	691	19	12.5
0031–07	416	10.9	39	400	96	–0.04	984	19	6.6
0031–07	750	10.9	35	672	29	1.09	1996	19	1.8
0136+57	310	72.2	40/2	2786	47	...	...	...	87.0
0136+57	750	72.2	36/2	2513	12	...	...	...	46.0
0138+59	310	34.8	36/2	578	54	–1.76	363	25	94.9
0138+59	416	34.8	38/2	80	31	–1.20	516	25	49.7
0138+59	750	34.8	28/2	498	14	–0.07	1047	25	13.6
0301+19	310	15.7	38	145	34	–1.26	148	48	12.2
0301+19	416	15.7	39	266	37	–0.70	210	48	6.4
0301+19	750	15.7	39	434	14	0.43	427	48	1.8
0329+54	310	26.8	38	242	1479	–1.65	138	68	28.0
0329+54	416	26.8	39	545	1639	–1.09	196	68	14.7
0329+54	750	26.8	39	890	921	0.04	398	68	4.0
0355+54	310	57.0	38	5207	62	–2.22	28	145	21.3
0355+54	416	57.0	37	2409	53	–1.66	40	145	11.1
0355+54	750	57.0	38	4512	33	–0.53	81	145	3.0
1508+55	310	19.6	33	569	162	–1.87	32	128	10.7
1508+55	416	19.6	32	431	96	–1.31	45	128	5.6
1508+55	750	19.6	31	805	26	–0.18	91	128	1.5
1541+09	416	35.0	32	513	61	–2.08	108	30	78.8
1541+09	750	35.0	28	838	19	–0.95	219	30	21.5
1604–00	310	10.7	34	1838	74	–0.53	645	21	9.9
1604–00	416	10.7	32	942	59	0.03	918	21	5.2
1604–00	750	10.7	30	1577	16	1.16	1862	21	1.4
1642–03	416	35.7	34	1028	305	–1.12	61	56	4.9
1642–03	750	35.7	35	1669	86	0.01	123	56	1.3
1706–16	310	24.9	32	657	47	–1.50	186	36	26.8
1706–16	416	24.9	32	590	47	–0.94	265	36	14.0
1706–16	750	24.9	33	961	25	0.19	537	36	3.8
1737+13	310	48.4	31	922	31	–1.94	41	144	16.1
1737+13	416	48.4	34	477	23	–1.38	58	144	8.4
1737+13	750	48.4	33	785	11	–0.25	118	144	2.3
1818–04	416	84.4	36	641	135	–3.73	7	69	237.9
1844–04	310	141.9	31	1083	69	...	...	...	258.0
1919+21	310	12.4	37	39	303	–0.86	141	65	4.6
1919+21	416	12.4	37	255	201	–0.30	201	65	2.4
1919+21	750	12.4	37	441	31	0.83	407	65	0.7
1933+16	310	158.5	40/2	2109	295	–4.04	8	120	395.7
1933+16	750	158.5	34/2	1311	130	–2.35	23	120	56.7
1944+17	310	16.3	36/2	1455	34	–1.48	282	18	38.7
1944+17	416	16.3	34/2	906	33	–0.92	401	18	20.2
1944+17	750	16.3	34/2	1489	22	0.21	813	18	5.5
2016+28	310	14.2	40/2	658	443	–1.44	436	20	54.6
2016+28	416	14.2	36/2	690	318	–0.88	621	20	28.6
2016+28	750	14.2	36/2	1138	55	0.25	1259	20	7.8
2020+28	310	24.6	42/2	320	122	–1.11	275	47	16.1
2020+28	416	24.6	40/2	1666	112	–0.55	392	47	8.4
2020+28	750	24.6	40/2	1888	58	0.58	794	47	2.3
2045–16	310	11.5	40	88	162	–0.54	63	214	1.0
2045–16	416	11.5	37	151	127	0.02	90	214	0.5
2045–16	750	11.5	38	330	67	1.15	182	214	0.1
2111+46	310	141.5	37	950	209	–3.86	13	80	414.4
2111+46	416	141.5	37	171	117	–3.30	18	80	217.0
2111+46	750	141.5	39	662	72	–2.17	36	80	59.3
2154+40	416	71.0	41	364	92	–2.39	11	298	15.7
2154+40	750	71.0	38	386	47	–1.26	21	298	4.3
2217+47	310	43.5	40	1336	318	–1.88	55	103	18.9
2217+47	416	43.5	39	748	135	–1.32	78	103	9.9
2217+47	750	43.5	41	1148	17	–0.19	159	103	2.7
2255+58	310	148.0	40	345	72	...	...	...	276
2255+58	416	148.0	39	1308	59	...	...	...	145
2255+58	750	148.0	38	1680	24	...	...	...	39
2319+60	310	96.0	42	495	68	–3.77	10	93	255.5
2319+60	416	96.0	41	104	59	–3.21	14	93	133.8
2319+60	750	96.0	41	418	36	–2.08	28	93	36.6

DMs, so that DISS caused large fractional fluctuations in the daily flux-density values measured for such objects.

b) Calibration

Daily calibration observations were made of the extragalactic sources 3C 33 and 3C 380. The source 3C 33 was chosen because it does not contain any compact component that might scintillate or vary intrinsically—its 430 MHz fringe visibility between Arecibo and Green Bank is $\gamma < 0.01$ (Broderick and Condon 1975). Whereas pulsar observations were made by tracking the pulsar position and allowing the periodic time variation of the pulsar to build up a profile, the steady calibration sources were observed with drift scans at two or three different hour angles. By setting the averaging period equal to the duration of the drift scan, we were able to use the signal averager to obtain calibrator data with the same

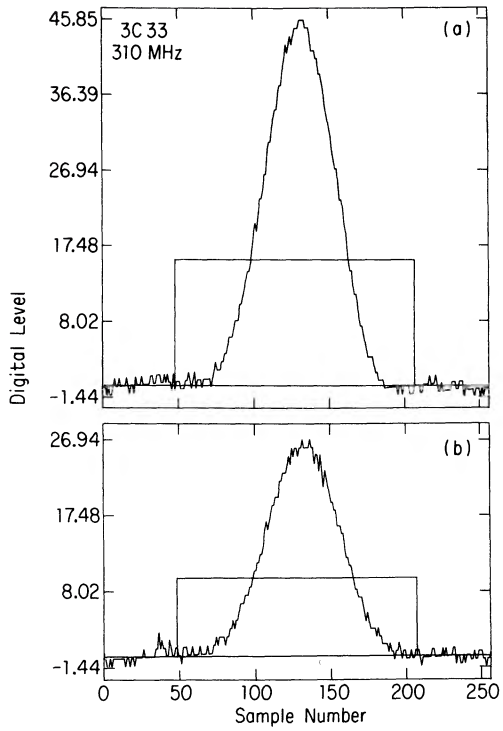

FIG. 2.—Results from a single scan of the extragalactic calibration source 3C 33 at 310 MHz. Panels (*a*) and (*b*) are orthogonal linear polarizations. It was observed with the same equipment and analyzed with the same programs as the pulsar scans (see Fig. 1). The abscissa is the sample number; the ordinate is the uncalibrated flux density (digital levels).

equipment and data format as those of the pulsars (see Fig. 2). Previous experience with the cooled upconverter receivers and analysis of the calibration data showed that receiver gain variations were typically less than 2% over the interval ($\approx$12 hr) between calibration scans.

The ultimate goal of our data reduction procedure was to obtain a set of scan-averaged total flux densities S_{pvi}, where the index p labels the pulsar; v, the frequency of observation; and i, the day of the observation. The first step in this procedure was to form 2048 point scan averages from the recorded 10 s averages. These 2048 point pulse profiles were passed through a digital filter that replaced each point with the median of itself and the four adjacent points on either side. This nine point median filter removed most impulsive interference from the data without significantly broadening the pulse profile. The phase of the pulse peak was found by cross-correlating the smoothed profile with a triangular function whose base width was about 10% wider than the known full width of the pulse at the 10% level. This cross-correlation was performed on the sum of the two polarization channels for maximum sensitivity. Once the phase of the pulse peak had been found, we shifted it to 180° and subtracted linear baselines from the two polarization channels separately. We then integrated across the pulse profiles to obtain the scan-averaged, uncalibrated (in units of digital levels) flux density $U_{pvi\pi}$ in each polarization channel π.

Plots of the calibration scans were measured by hand. A linear baseline was fitted to each, and the peak deflection (again, in digital levels from the signal averager) was recorded for each polarization channel. Time series of these deflections reveal slow (5–10 day) drifts in the overall system gain at about the 10% level. These purely time-dependent gain variations G_i were approximated by a smooth function fitted to the time series. Since the calibration drift scans were made at several different hour angles, we were also able to measure the telescope gain as a function of hour angle, G_h. We need to know G_h only approximately since all observations of a particular pulsar were always made over the same hour-angle ranges on successive days. Then, using assumed flux densities for both calibration sources at each of the three frequencies (see Table 2), we determined the six time-independent gain constants $G_{v\pi}$ (with dimensions of digital levels per Jy) needed to characterize the average on-axis gains for both polarizations π at all three observing frequencies v. The results of the calibration are shown in Table 2 and Figures 3 and 4. At 310 MHz and 750 MHz the rms scatter of the calibrator flux densities is about 4%. The 416 MHz data, with a scatter of 7%, was noisier throughout the observing session, particularly in one of the polarization channels. These fluctuations were partly due to decreased sensitivity of this channel because the feed was being operated near the end of its frequency range. Because both the pulsars and calibration sources were observed with the same equipment, we believe that the pulsar calibration uncertainties are also only 4% at 310 MHz and 750 MHz, and 7% at 416 MHz.

The uncalibrated pulsar flux densities were then scaled by the gain values derived from the calibration scans. We averaged the pulsar flux densities from the two polarization channels to form the total intensities

$$S_{pvi} = (\tfrac{1}{2}) G_i^{-1} G_h^{-1} \sum_{\pi=1}^{2} U_{pvi\pi} G_{v\pi}^{-1} , \quad (1)$$

which are the basis of our scintillation analysis. Once this automated processing was completed, the entire set of raw data plots was rechecked for interference, bad baselines, or other problems. Bad scans were either reanalyzed by hand or deleted from the data set.

Since pulsar radiation is very often highly linearly polarized, time-varying Faraday rotation in the ionosphere can cause large intensity variations in the separate polarization channels. This effect does not influence the accuracy of the total-intensity measurements, however.

c) *Data Presentation: Time Series and Structure Functions*

We present our results in two formats. First, we plot flux-density time series on logarithmic scales in order to make it easier to compare percentage flux variations at different flux levels. The mean flux levels are recorded in Table 1. Since the flux scale is logarithmic, the mean ordinate value is unimportant and has been chosen to clarify the presentation.

The second format consists of structure function plots of

TABLE 2

SUMMARY OF CALIBRATOR OBSERVATIONS

Source	v (MHz)	Assumed Flux Density (Jy)	Observed Flux Density (Jy)	m_{obs}
3C 33	310	37.0	35.4	4.6%
	416	29.0	30.7	7.8
	750	20.0	19.9	4.9
3C 380	310	41.0	39.7	4.0
	416	34.0	34.0	8.0
	750	21.0	20.9	3.7

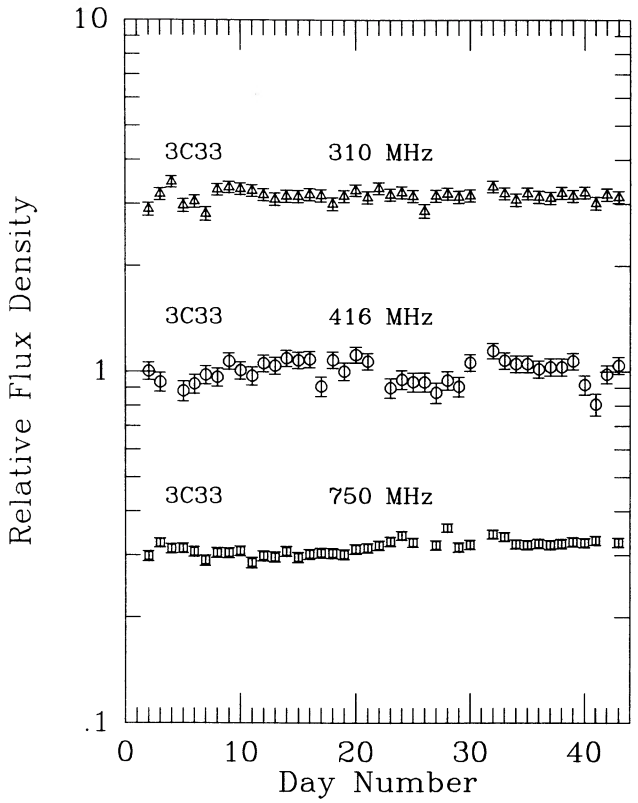

FIG. 3a

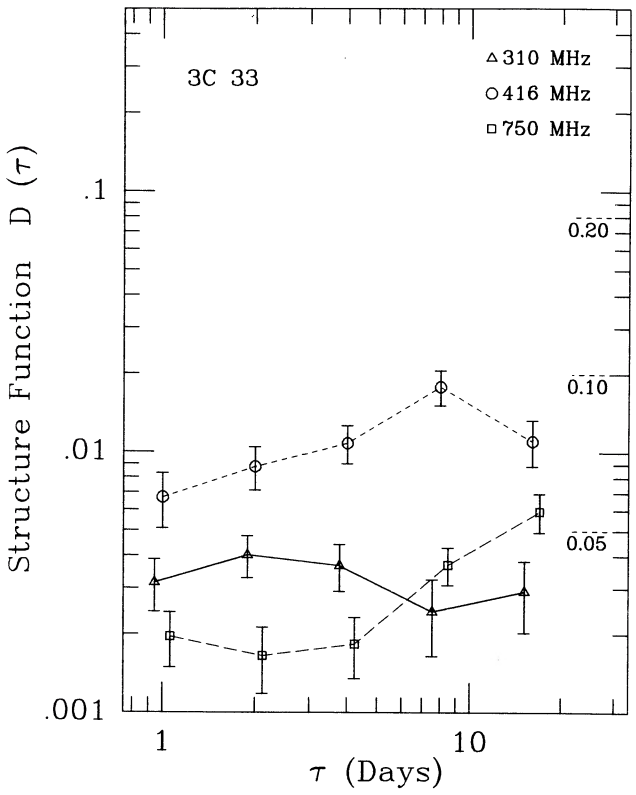

FIG. 3b

FIG. 3.—(*a*) Light curves of the calibration source 3C 33 at 310 MHz (*triangles*), 416 MHz (*circles*), and 750 MHz (*squares*). The rms scatter of individual points about their mean is 4% at 310 and 750 MHz, 7% at 416 MHz. The flux densities are plotted on logarithmic scales to facilitate comparisons of fractional flux-density changes and shifted vertically for clarity. The error bars span ± 2 standard errors ($\approx 95\%$ confidence interval). (*b*) Structure function plots for the time series in (*a*), with the same data symbols. The structure function values are plotted at lags of $\tau = 1, 2, 4, 8$, and 16 days with $\pm 1\ \sigma$ error bars. Modulation index levels $m = 0.05$, 0.10, and 0.20 are shown on the right-hand axis for comparison. Both axes are logarithmic. See § IIc for a further discussion of structure functions and their interpretation.

selected time series. Structure functions have been used extensively in the study of scintillation, turbulence in random media, and the characterization of oscillator stability (see Simonetti, Cordes, and Heeschen 1985, and references therein). The first-order structure function, the only one we use here, is defined as

$$D(\tau) \equiv D_{pv}^{(1)}(\tau) = \frac{1}{N(\tau)\bar{x}^2} \sum_{i=1}^{N-\tau} (x_{i+\tau} - x_i)^2 , \qquad (2)$$

where $x_i = S_{pvi}$, $\bar{x}$ is the sample mean, and τ is discrete in units of the sampling interval = 1 day, N is the number of samples, and $N(k)$ is a normalizing factor equal to the number of observations included in the sum. For a stationary time series with finite variance $D(\tau) = 2\sigma^2[1 - \rho(\tau)]/\bar{x}^2$ in the limit of an infinitely long data span, where $\rho(\tau)$ is the autocovariance function and σ^2 is the variance.

A structure function will normally display three distinct regimes of behavior, as illustrated schematically in Figure 5. In the "noise regime" ($\tau \ll \tau_1$), uncorrelated sources of noise dominate any correlated variation of the time series. The structure function takes on a constant value of $2\sigma_n^2$ throughout this regime, where σ_n^2 is the noise variance. In the "structure regime" ($\tau_1 < \tau < \tau_2$), the structure function monotonically increases with τ at a rate determined by the slope of the autocovariance function at that lag. Finally, when τ is significantly longer than the longest time scale for variation in the process, τ_2, the structure function reaches the "saturation regime" characterized by a constant value of $2\sigma_t^2$, where $\sigma_t^2 = \sigma_n^2 + \sigma_c^2$ represents the total variance of the time series including all sources of noise and all correlated variations. Many naturally occurring time series have a region of approximately power-law increase in the structure regime, making log-log plots of structure functions useful in determining the slope of the power law. Note that the slope of the first-order structure function is unaffected by misestimating the mean μ of the underlying process [although all the values of $D(\tau)$ will be scaled by $\bar{x}^2/\mu^2$]. A linear trend in a time series will result in a logarithmic slope of 2 for the first-order structure function in the structure regime.

d) Noiselike Fluctuations

Noiselike processes raise the overall level of the structure function without introducing any net trend. Noise decreases the sensitivity of the structure functions to correlated structure in the time series by raising the baseline level of $D(\tau)$ and increasing its estimation error. We have identified four noiselike processes in our observations.

Calibration noise, due to imperfect knowledge of receiver and antenna gains, introduces a constant fractional error in the flux measurements. By reference to the calibrator sources in Table 2, we estimate the fractional errors in the calibration to be $\epsilon_c = 0.04$ at 310 MHz, 0.07 at 416 MHz, and 0.04 at 750 MHz.

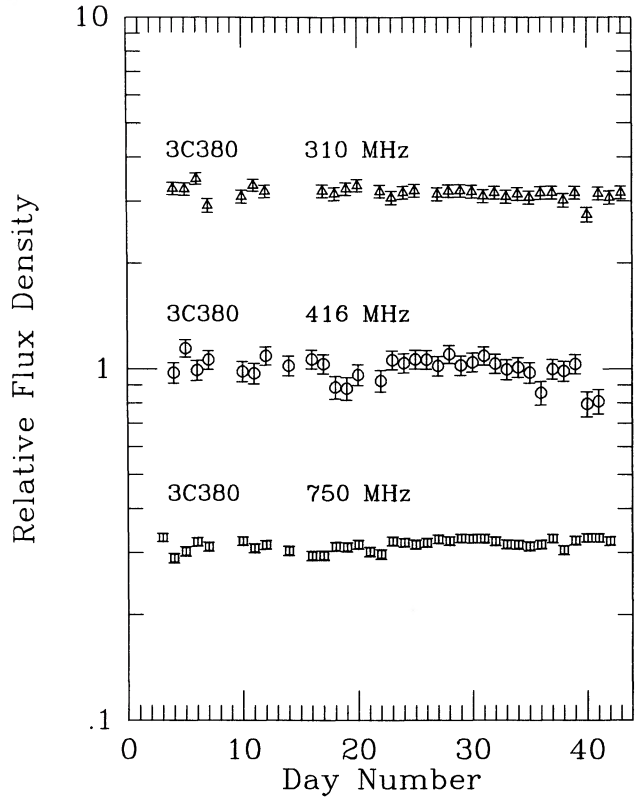

FIG. 4a

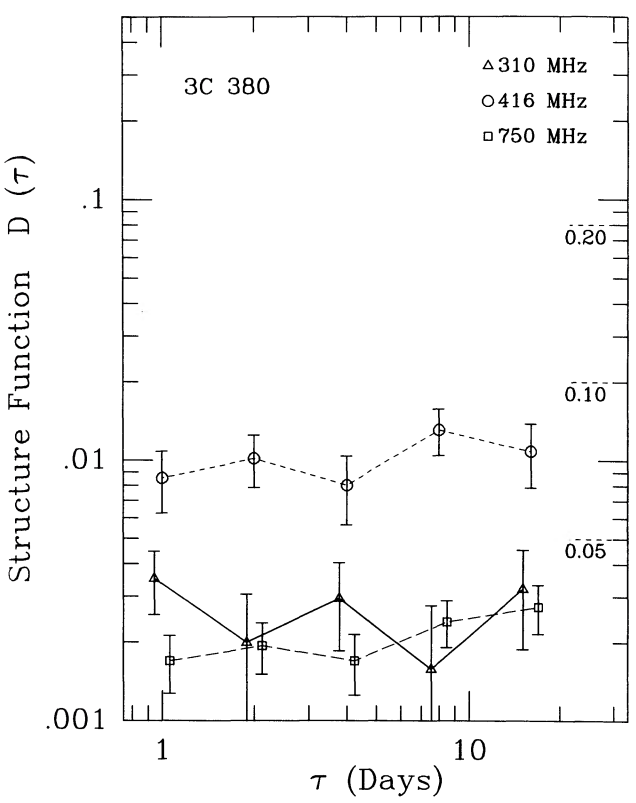

FIG. 4b

FIG. 4.—(*a*) Light curves of the calibration source 3C 380 at 310 MHz (*triangles*), 416 MHz (*circles*), and 750 MHz (*squares*). (*b*) Structure function plots for the time series in (*a*), with the same data symbols.

Measurement noise is due to the finite signal-to-noise ratio of the average pulse profile accumulated during the scan. For an N point profile with n points of signal and $N - n$ points of baseline, the fractional error in estimating the flux is $\epsilon_m = (\sigma_b/S)[(N/n)/(N-n)]^{1/2}$, where σ_b is the rms noise over the baseline region and S is the continuum flux, $S = (1/N)\sum_{i=1}^{N} S_i$. The values for ϵ_m for each scan were determined and combined quadratically to form an average value of $D_m = 2\epsilon_m^2$, the contribution of measurement error to the structure function value. Table 3 contains values of ϵ_m for the noise-dominated time series.

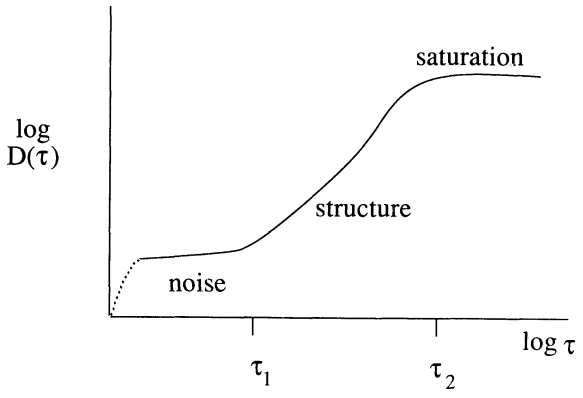

FIG. 5.—Structure function (schematic) for a process with fluctuations on time scales $\tau_1 < \tau < \tau_2$. In the *noise regime* ($\tau < \tau_1$), no correlated fluctuations are present and the structure function is flat. In the *structure regime* ($\tau_1 < \tau < \tau_2$), $D(\tau)$ monotonically increases with a slope which depends on the power spectrum of the correlated fluctuations. Many naturally occurring processes exhibit power-law increases in this regime. In the *saturation regime* ($\tau > \tau_2$), the structure function attains its maximum and constant value of $2\sigma^2$, where $\sigma^2 = \sigma_n^2 + \sigma_c^2$, with σ_n^2 and σ_c^2 the variances of the noiselike and correlated portion of the process, respectively. A nonstationary random process has an infinite value of τ_2 and $D(\tau)$ increases without bound for large τ. The dashed line near the origin is meant to indicate that $D(0) = 0$, showing that the noise decorrelates rapidly compared to the signal.

Stabilization noise is due to the finite number of pulses included in the average profile. Individual pulses are highly variable in shape and strength. The modulation index of pulsar average profiles has been studied by Weisberg *et al.* (1986) and others. They find that the pulse-to-pulse modulation index m_{pp} varies with position across the average profile, but is generally within the range $0.5 \leq m_{pp} \leq 2.0$. We estimate the fractional error in the flux estimate due to stabilization noise as $\epsilon_s = m_{pp}/M^{1/2}$, where M is the number of pulses observed in a scan. The mean value of M for each pulsar and observing frequency is given in Table 1. Values of $D_s = 2\epsilon_s^2$ are tabulated in Table 3.

DISS noise is the fourth and often dominant noiselike process in the observations. Diffractive scintillation has a time scale T_d and a frequency scale $\Delta\nu_d$. DISS has a modulation index ≥ 1.0, leading to a fractional flux error of $\epsilon_d \approx 1/N_{\rm scint}^{1/2}$, where $N_{\rm scint}$ is the number of independent scintillation maxima in the observation. The number of scintillation maxima is $N_{\rm scint} = f_d(\Delta t\,\Delta\nu)/(T_d\,\Delta\nu_d)$ for an observation of duration Δt and a bandwidth of $\Delta\nu$. The filling factor $f_d \approx 0.20$ accounts for the fact that the scintillation maxima fill only a fraction of the frequency-time plane. This simplified estimate does not account for the details of the DISS statistics or the fact that DISS often exhibits correlated structure in the frequency-time

TABLE 3

NOISE-DOMINATED TIME SERIES

PSR	ν (MHz)	D_m (log)	D_s (log)	D_d (log)	D_{noise} (log)	<D(τ)> (log)	m_{obs}	T_r (days)
0031-07	310	-3.68	-2.52	0.07	0.08	0.22	0.91	12
0031-07	416	-2.61	-2.30	0.98	0.98	0.17	0.86	6.6
0031-07	750	-3.17	-2.53	1.61	1.61	0.37	1.09	1.8
0136+57	310	-2.92	--3.15	4.04	-2.28	-1.67	0.10	87
0136+57	750	-2.69	--3.10	2.45	-2.02	-1.60	0.11	46
0138+59	310	-3.25	--2.46	1.42	-1.35	-1.07	0.21	95
0138+59	416	-1.49	-1.60	0.12	0.14	-0.78	0.29	50
0138+59	750	-2.44	-2.40	0.19	0.19	-0.80	0.28	14
0301+19	750	-2.48	-2.34	0.31	0.31	-0.06	0.66	1.8
0355+54	750	-3.16	--3.35	1.44	-1.39	-0.72	0.31	3.0
1508+55	310	-2.93	--2.45	2.37	-1.91	-0.95	0.24	11
1508+55	416	-3.04	--2.33	1.56	-1.37	-0.89	0.25	5.6
1508+55	750	-3.07	--2.60	0.97	-0.94	-0.65	0.33	1.5
1541+09	416	-2.23	--2.41	2.03	-1.54	-1.28	0.16	79
1541+09	750	-2.37	--2.62	1.38	-1.29	-1.05	0.21	22
1604-00	310	-3.22	-2.96	0.02	0.02	-0.44	0.43	9.9
1604-00	416	-1.91	-2.67	1.00	1.00	0.33	1.04	5.2
1604-00	750	-2.82	-2.90	1.63	1.63	0.35	1.06	1.4
1642-03	416	-3.88	--2.71	1.33	-1.24	-0.01	0.70	4.9
1642-03	750	-4.29	--2.92	0.69	-0.68	0.17	0.86	1.3
1706-16	310	-2.93	--2.52	1.24	-1.18	-0.78	0.29	27
1706-16	416	-2.32	--2.47	0.50	-0.48	-1.03	0.22	14
1706-16	750	-3.18	-2.68	0.15	0.15	-0.19	0.57	3.8
1737+13	310	-2.37	--2.66	2.57	-1.91	-1.05	0.21	16
1737+13	750	-1.99	--2.59	0.95	-0.90	-0.23	0.54	2.3
1818-04	416	-3.05	--2.51	4.85	-1.86	-1.84	0.08	240
1919+21	310	-3.60	-1.30	0.19	0.21	-0.03	0.69	4.6
1919+21	416	-3.78	-2.11	0.07	0.08	0.11	0.80	2.4
1919+21	750	-3.47	-2.34	0.70	0.70	0.27	0.97	0.7
1933+16	310	-3.81	--3.02	5.39	-2.37	-2.40	0.04	400
1944+17	310	-2.55	--2.86	1.21	-1.16	-0.78	0.29	39
1944+17	416	-2.23	--2.66	0.32	-0.30	-0.67	0.33	20
1944+17	750	-3.04	-2.87	0.33	0.33	-0.49	0.40	5.5
2016+28	310	-4.37	--2.52	0.74	-0.72	-1.18	0.18	55
2016+28	416	-3.87	--2.54	0.07	-0.06	-1.04	0.21	29
2016+28	750	-4.09	-2.76	0.57	0.57	-0.60	0.35	7.8
2020+28	310	-3.36	--2.20	0.08	-0.08	-0.53	0.38	16
2020+28	416	-3.58	--2.92	0.11	-0.11	-0.25	0.53	8.4
2020+28	750	-4.12	-2.98	0.69	0.69	-0.31	0.50	2.3
2045-16	310	-3.69	--1.64	0.35	-0.33	-0.15	0.60	1.0
2045-16	416	-3.08	-1.88	0.10	0.11	0.12	0.81	0.5
2045-16	750	-3.60	-2.22	0.62	0.63	0.48	1.23	0.1
2111+46	310	-4.04	--2.68	5.12	-2.27	-2.49	0.04	410
2111+46	416	-2.78	--1.93	3.68	-1.63	-1.32	0.16	220
2111+46	750	-3.51	--2.52	3.41	-2.16	-1.82	0.09	60
2217+47	750	-3.03	--2.76	0.76	-0.74	-0.85	0.27	2.7
2255+58	310	-1.50	--2.24	4.92	-1.39	-1.03	0.22	280
2255+58	416	-1.10	--2.82	4.81	-1.04	-1.47	0.13	150
2319+60	310	-3.10	--2.39	5.21	-2.09	-1.34	0.15	260
2319+60	416	-2.18	--1.72	3.84	-1.45	-0.83	0.27	130
2319+60	750	-3.04	--2.32	3.59	-2.04	-1.56	0.12	37

plane, but, lacking more detailed information about the DISS behavior, we will use this expression for ϵ_d to estimate the error introduced by diffractive scintillation. In calculating ϵ_d we have used the DISS parameters found by Cordes, Weisberg, and Boriakoff (1985) scaled to our observing frequencies as $T_d \propto \nu^{1.2}$ and $\Delta\nu_d \propto \nu^{4.4}$, the scaling appropriate for a Kolmogorov spectrum (see the Appendix). The scaled DISS parameters are given in Table 1 and $D_d = 2\epsilon_d^2$ is shown in Table 3.

Since these noise sources are independent, their cumulative effect on $D(\tau)$ will be to raise all values in a time series by a constant amount $D_{\rm noise} = 2(\epsilon_c^2 + \epsilon_m^2 + \epsilon_s^2 + \epsilon_d^2)$, which is tabulated in Table 3. Although this is our best estimate of the total noise present in the observations, difficulty in estimating stabilization noise and DISS noise may result in a misestimate of $D_{\rm noise}$ by as much as a factor of 10 in either direction. An observed noise level that is smaller than expected is not serious since it merely indicates an overestimate of $D_{\rm noise}$. An observed noise level that is larger than expected is a problem, however, since it is impossible to tell whether the estimate of $D_{\rm noise}$ is in error, whether there is an unsuspected source of additional noise in the system, or whether the pulsar is displaying day-to-day variability that would show up as an additional source of noise. We have investigated the effect that changing the assumed values of $m_{\rm pp}$ or f_d have on the error estimates. For $m_{\rm pp} = 1$ and $f_d = 0.20$ this noise ratio varies between 0.05 and 20 with a median value of 0.86. The distribution of this noise ratio, which is sensitive to the choice of f_d but not to $m_{\rm pp}$ (because DISS noise dominates over stabilization noise in most cases), clearly becomes biased when f_d deviates from 0.20 by more than a factor of 2. Although individual noise estimates can vary by more than a factor of 10 from the observed values, there is no obvious bias or trend in the error estimates.

The structure function values, like those of the autocovariance function, are highly correlated for lags separated by less than an octave and are still partially correlated over a number of octaves. This is why we have chosen to plot only the $\tau = 1$, 2, 4, 8, and 16 day lag values of the structure function. The error bars on those points are $\pm 1\sigma_D$, where $\sigma_D^2 \approx 8\sigma_n^2 D(\tau)/N(k)$ is the estimator of the structure function variance (Simonetti, Cordes, and Heeschen 1985) and σ_n^2 is the noise

variance. Although we have attempted to account for all sources of noise in the measurements, uncertainty in the estimates of stabilization noise and DISS noise make the calculated error estimates uncertain. We have therefore estimated the noise by using the shortest available lag of the structure function ($\tau = 1$ or 2 days), $\sigma_n^2 \equiv D(1)/2$. This will be an overestimate of the error for a few time series, such as PSR 1933+16, which have structure functions that are still sharply decreasing at the shortest available lag.

III. RESULTS

a) *Pulsars Are Stable Continuum Sources*

Many of the time series in our observations are noiselike; that is, they exhibit no correlated structure in the time domain and have essentially flat structure functions. Table 3 summarizes the results for these data sets, listing the estimated noise contribution, $D_{\rm noise}$, the observed mean structure function value, $\langle D(\tau)\rangle$, the observed modulation index, $m_{\rm obs} = [\langle D(\tau)\rangle/2]^{1/2}$, and the calculated refractive time scale, T_r. A time series in our observations will be noiselike if any refractive scintillation modulation is small compared to the sources of noise or if T_r is comparable to or shorter than the 1 day spacing of our flux measurements. This latter condition blends diffractive and refractive effects so thoroughly that no useful information about RISS can be extracted from the time series. The time series will also be noiselike if the duration of the observations is much less than T_r. In this case, if the intrinsic flux density of the pulsar is constant, we will observe a roughly constant flux density contaminated by some amount of additive noise. On the other hand, if pulsars are not constant flux sources on the time scale that we are probing (minutes to weeks), then we can expect that there will be additional fluctuations in the time series above the level of the noise that we have accounted for.

In Figure 6 we have plotted the observed modulation index, $m_{\rm obs}$ against our best estimate of the noise contribution to the modulation index $m_{\rm noise} = [D(\tau)/2]^{1/2}$ for the 51 time series in Table 3. Those time series that lie below and to the right of the dashed line are contaminated by noise contributions, since their estimated $m_{\rm noise}$ is greater than $m_{\rm obs}$. Not surprisingly, these points are mainly from the time series for which T_r is less than or comparable to the duration of our observations, since a small value of T_r indicates that the diffractive time scale T_d is becoming long and the diffractive bandwidth is also becoming large. The points with $T_r < 10$ days to the left and above the dashed line are probably also corrupted by DISS noise, and we have underestimated its contribution to the noise total. We see in Figure 6 that the time series with intermediate refractive time scales ($10 \leq T_r < 100$ days) and minimal noise corruption have modulation indices no larger than about 0.3. This is important because it indicates that the modulation index of RISS is relatively small since at least some of the uncorrupted time series in this group would show large $m_{\rm obs}$ otherwise. The time series with the longest values of T_r show the smallest values of $m_{\rm obs}$ as would be expected if these pulsars are intrinsically stable and the RISS modulation is reduced by the small duration of our observations relative to T_r for these data.

This point is explored further in Figure 7. There we have plotted $m_{\rm obs}$ against T_r for the 51 time series in Table 3. The tendency for time series with large T_r to have small modulation indices is clear in this figure. Most of the points in the lower right-hand corner of this figure have very low $m_{\rm noise}$ values. For

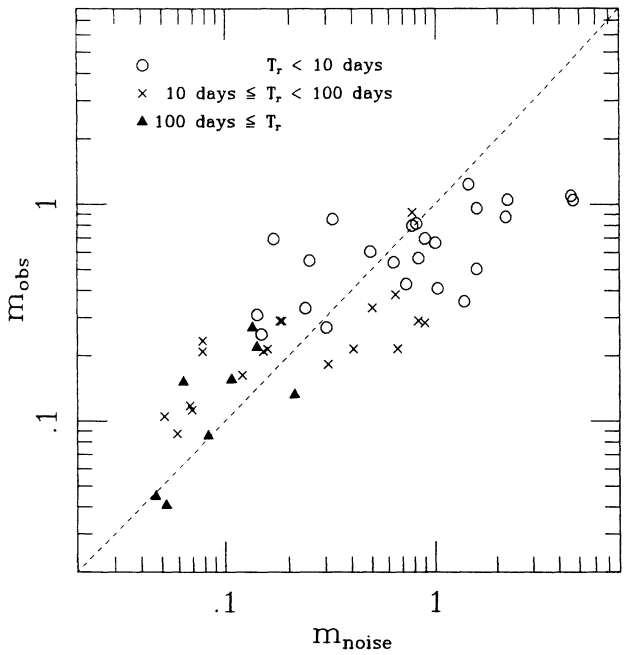

FIG. 6.—Observed modulation index plotted against the modulation index estimated from noise statistics. Points falling below and to the right of the dashed line are contaminated by noise and are not reliable estimates of the RISS modulation depth. The points are also split into three groups based on the expected refractive time scale for that pulsar and observing frequency. The general agreement with RISS theory is evident, with those time series with large T_r values exhibiting very low values of $m_{\rm obs}$ and those with intermediate T_r values exhibiting modulation indices in the range 0.2–0.3.

them to then also have low observed modulation indices (as low as the continuum calibrators in some cases) requires that intrinsic pulsar variability must be very small for these pulsars. For the most extreme cases we can set limits of $m_{\rm psr} \leq 0.05$ for intrinsic pulsar variability over our 40 day observing span.

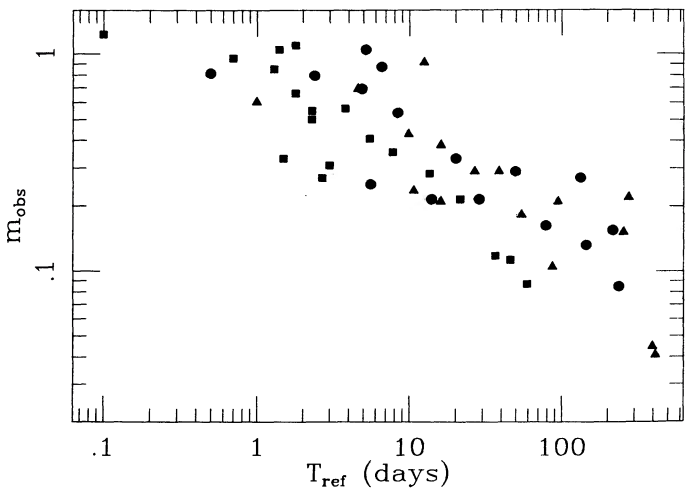

FIG. 7.—Observed modulation indices plotted against the expected refractive time scale T_r for 51 time series showing noiselike behavior. Different observing frequencies are denoted by triangles (310 MHz), circles (416 MHz), and squares (750 MHz). The trend for large T_r value data to show very low modulation is evident. This is consistent with RISS theory and furthermore indicates that pulsars are stable continuum sources over this time span (40 days).

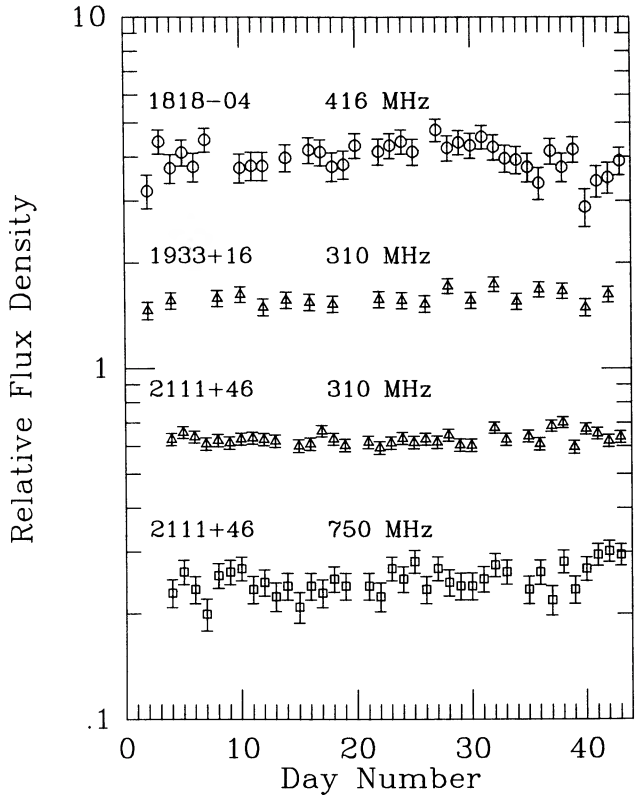

FIG. 8a

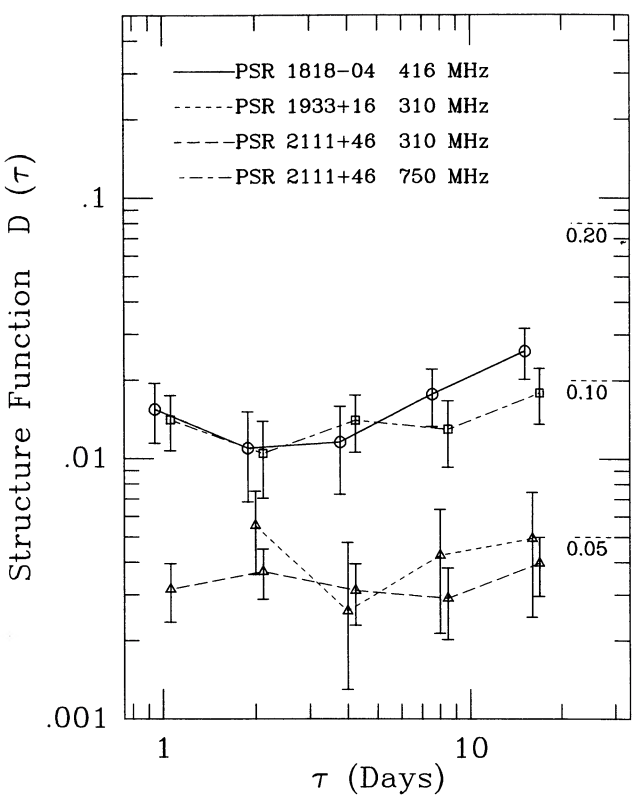

FIG. 8b

FIG. 8.—(*a*) Pulsar time series with flux values nearly as stable as the calibrator sources. The value of T_r for these sources is $\gg 43$ days. (*b*) Structure functions for the same sources as in (*a*). Data symbols as in Figs. 3 and 4.

Four of the most stable pulsar time series are displayed in Figure 8 along with their structure functions. The lack of any significant increase in the $D(\tau)$ level above that due to calibration noise sets upper bounds on the intrinsic modulation depth, $m_{\rm int}$, of $m_{\rm int} \leq 0.04$ at 310 MHz, $m_{\rm int} \leq 0.07$ at 416 MHz, and $m_{\rm int} \leq 0.04$ at 750 MHz for the intrinsic intensity fluctuations of these pulsars over all time scales from several minutes to 40 days. The PSR 2111+46 time data at 750 MHz has a value of $m_{\rm obs}$ of 0.09. Since noise and intrinsic contributions will add linearly to the $D(\tau)$ value, data for this time series set a 3 σ limit of $m_{\rm int} \leq 0.16$ for the intrinsic variability of this pulsar at 750 MHz over the sampled time scales.

The predicted values of T_r for three of these time series are longer than 200 days (see Table 1). We note also that only one time series with $T_r > 100$ days shows any nonrandom intensity fluctuations (see § III*b*), and its T_r value is poorly determined because of a lack of DISS data. Since the value of T_r for a particular time series is dependent only on DISS parameters and the observing frequency, there is no reason to expect a correlation between RISS variability and intrinsic pulsar variability. The lack of any significant variability above the expected noise level for time series with large T_r values leads us to conclude that *pulsars are stable continuum sources on time scales of several minutes to several weeks.*

b) Refractive Scintillation: Times Scales

We turn now to a discussion of the time series in our data set which exhibit correlated intensity fluctuations. We identify correlated fluctuations by inspecting the structure function for the time series. Significant deviations from a constant value in the structure function indicate that there is correlated structure in the time series that is larger than that due to the noiselike (uncorrelated) component. We present time series and structure function pairs for nine such pulsars in Figures 9–12. These time series have a number of features in common. By selection, they all have structure functions that increase toward longer lags. This increase is usually monotonic, although there are instances of dips at a single lag value that are consistent with the estimation error of the structure functions (e.g., PSR 1737+13). Second, at shorter lag values many of the structure functions show evidence of contamination by noise. This has the effect of increasing $D(\tau)$ by a constant amount. This, in turn, flattens the slope of the structure function in this log-log presentation, since the $D(\tau)$ values on the left end of the curve are pushed upward proportionately more than those on the right end.

It would be useful to estimate RISS time scales from these structure functions in order to compare the observed values with T_r predicted by equations (A4) and (A12). We have not been able to do so with these data, however, since the separation between diffractive and refractive time scales is not great enough for those time series of most interest—namely, those which have T_r values between 10 and 30 days. At the short end of this range, the DISS decorrelation bandwidths $\Delta\nu_d$ and time scales T_d become large enough that our bandwidth and integration time per observation were inadequate to quench the DISS fluctuations fully. At the other end of this range, the RISS time scale starts to approach the total duration of our observation and the structure function estimates become unreliable. Our observations could be improved upon by using very wide

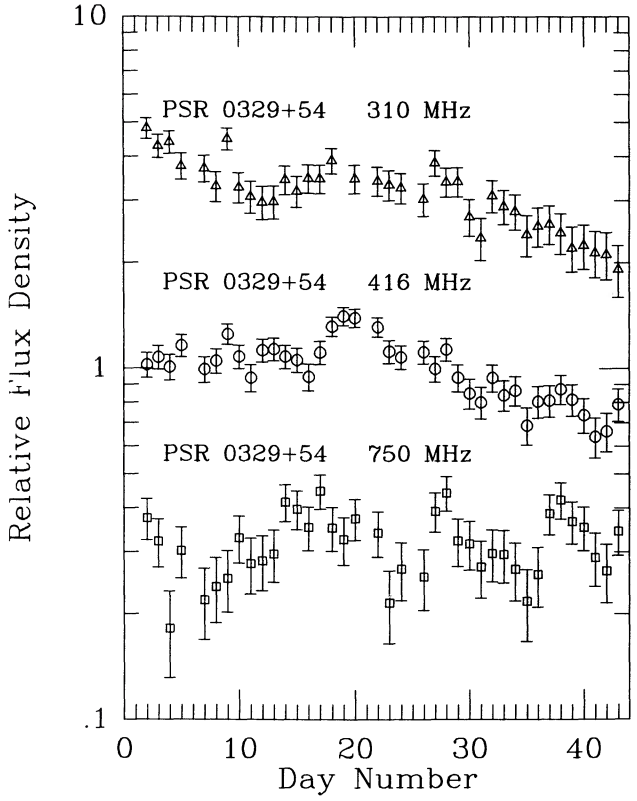

FIG. 9a

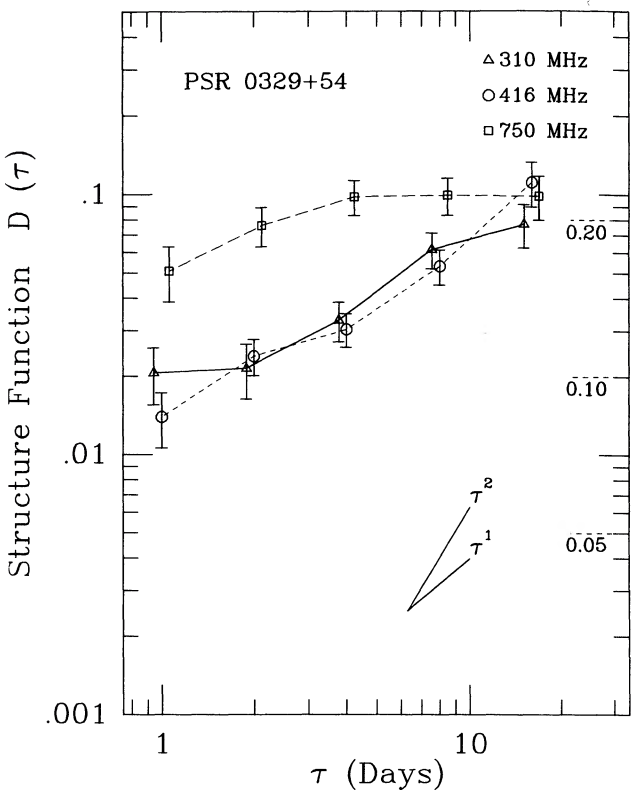

FIG. 9b

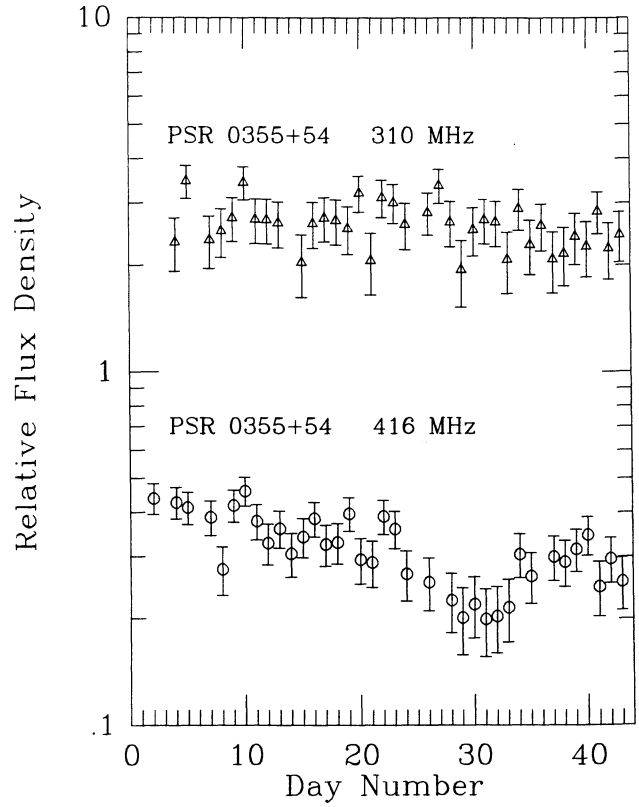

FIG. 10a

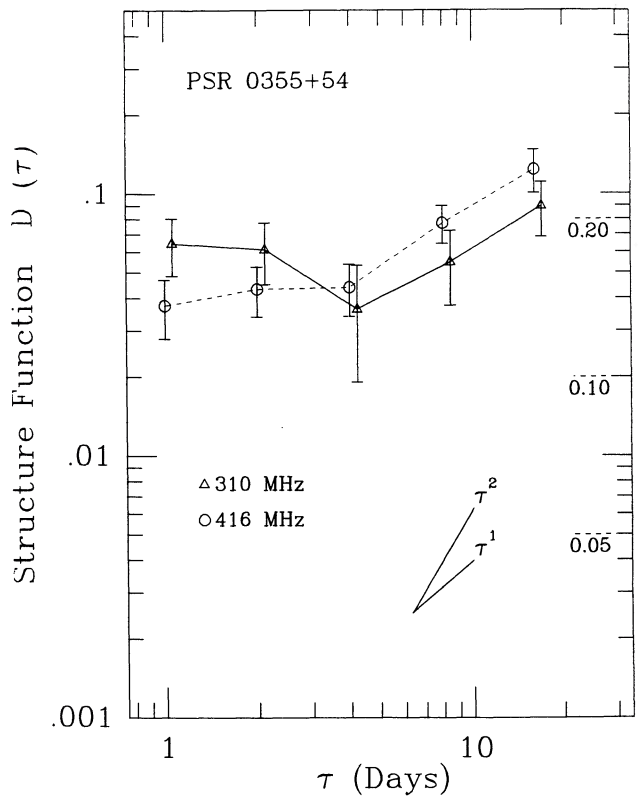

FIG. 10b

FIGS. 9–12.—(*a*) Light curves of six pulsars displaying refractive interstellar scintillation (RISS) behavior at one or more frequencies. The flux density time series are plotted on logarithmic scales to facilitate comparisons of fractional flux-density changes and shifted vertically for clarity. The error bars span ±2 standard errors. Data symbols as in Figs. 3 and 4. (*b*) Structure function plots for the time series in (*a*), with the same data symbols. Logarithmic slopes of 1 and 2 are identified.

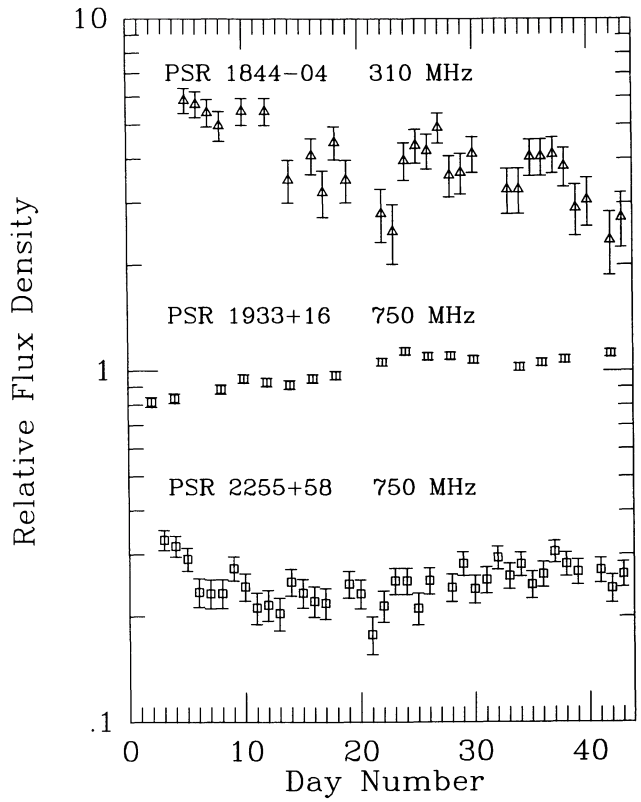

FIG. 11*a*

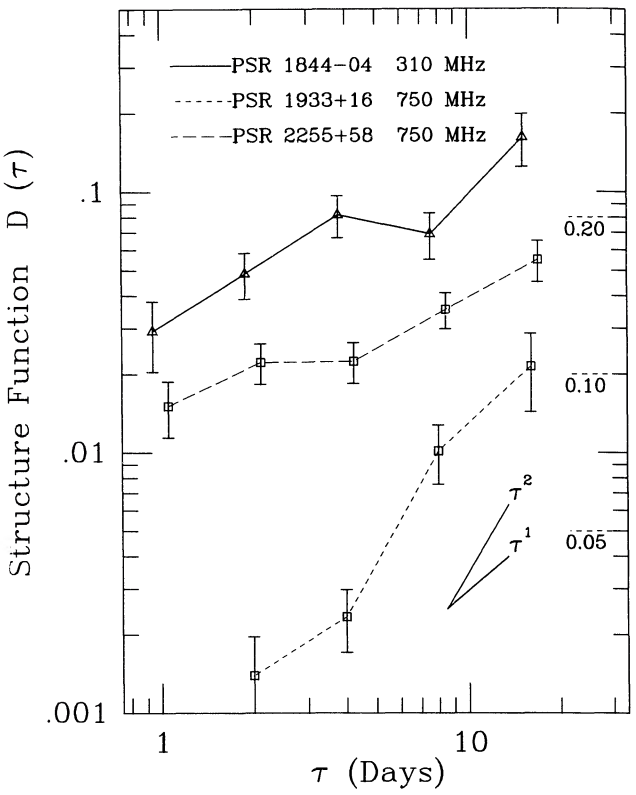

FIG. 11*b*

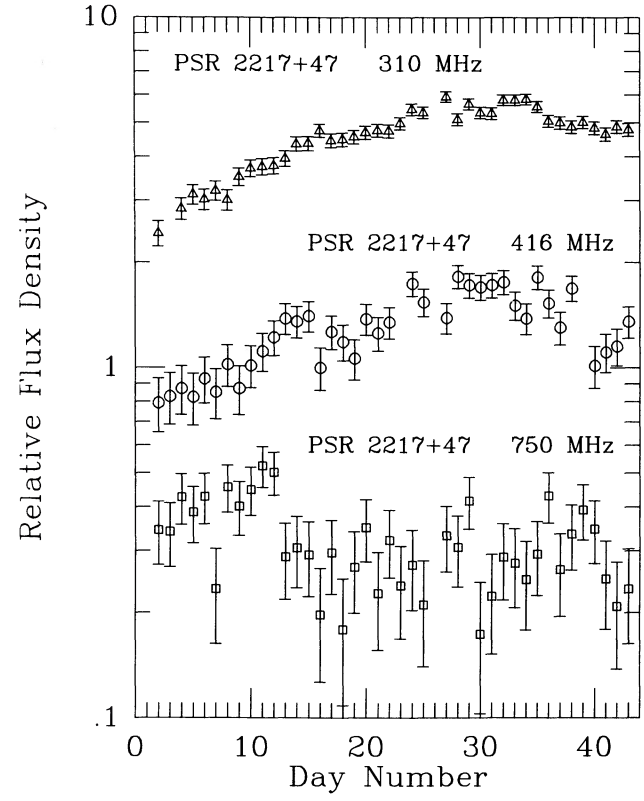

FIG. 12*a*

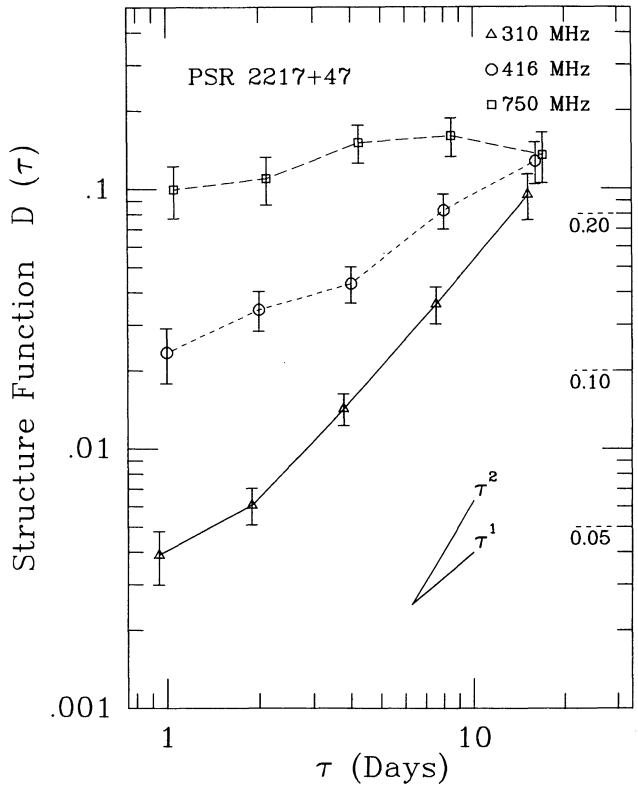

FIG. 12*b*

observing bandwidths (perhaps with interference rejection within the band), longer scans, and longer total duration.

Nevertheless, we can comment on the qualitative agreement between RISS theory and these observations. With one exception, the 11 time series which show RISS behavior in our observations have predicted values of $4 < T_r < 56$ days. The excellent qualitative agreement between the T_r values predicted by RISS theory and those observed in our experiment are support for the basic correctness of the theory.

The exception, PSR 1844−04 at 310 MHz, has a predicted value of 258 days based on the expression of Rickett, Coles, and Bourgois (1984), $T_r = 0.1\ \mathrm{DM}^{1.6}\lambda^{2.2}/V_{100}$ [days], where V_{100} is the pulsar transverse velocity in units of 100 km s^{-1}. This equation with $V_{100} = 1$ was used because of the lack of DISS parameters for this pulsar. T_r would be smaller for this source, and it would be in closer agreement with the other RISS results, if its velocity were larger than the median of the pulsar population. This same expression was used in determining T_r for PSR 0136+57 and PSR 2255+58 since no published DISS data for them exists.

We close this section with a brief discussion of the RISS behavior of the 11 time series and corresponding structure functions plotted in Figures 9–12. The predicted and observed values of D_{noise} are presented in Table 4, with some other parameters that will be discussed further below.

PSR 0329+54 (*Figs. 9a, b*).—This is an excellent example of RISS at all three observing frequencies, with the shortest time scales present in the 416 MHz and 750 MHz data and the longest time scale (to be compared with $T_r = 28$ days) at 310 MHz. At all three frequencies the modulation depth approaches 0.20 at the longest lags.

PSR 0355+54 (*Figs. 10a, b*).—RISS is evident at both frequencies although the 310 MHz data is affected by noise. The predicted value of $T_r = 11$ days agrees qualitatively with the behavior of the 416 MHz time series.

PSR 1844−04 (*Figs. 11a, b*).—The 310 MHz data is a good example of RISS behavior that has significant fluctuation power on time scales longer than 40 days. The structure function, which is only slightly affected by noise at the shorter lags, is showing no sign of saturation at the longest lag plotted here. This is in keeping with the net linear trend in the time series.

PSR 1933+16 (*Figs. 11a, b*).—This time series contains some of the quietest data obtained in these observations. There is a quasi-linear trend over the course of the observations. This is consistent with the $T_r = 57$ day value, although it looks like there are time scales present in the time series that are significantly longer than this. The structure function rises at almost the $D(\tau) \propto \tau^2$ behavior expected for a purely linear trend in the data.

PSR 2225+58 (*Figs. 11a, b*).—Although partially contaminated by noise, this time series shows substantial fluctuation power on 10–15 day time scales. Again, there is no indication that the structure function has saturated at the longest lag plotted here.

PSR 2217+47 (*Figs. 12a, b*).—These are the best examples of RISS behavior in the entire data set. The 310 MHz and 416 MHz data show strong long-term trends in the time series, although the calculated T_r values of 19 and 10 days, respectively, seem short compared to some of the time scales present in the data. Furthermore, there is a strong correlation between flux variations at the two frequencies. Such a wide-band correlation of flux variations was also seen in the observations of Hesse (1972) and is consistent with the wideband character of fluctuations expected from RISS. Refractive scintillation is also present in the 750 MHz data, but that time series is contaminated by noise.

c) *Refractive Scintillation: Modulation Index*

From Figures 6 and 7 it is clear that the maximum unambiguous RISS modulation index is not much larger than 0.30 in our data. It is possible, of course, that we may be missing some time series with larger values of m_r because of the limited duration of our observations and because of noise contamination for series with low values of T_r. However, even the time series with intermediate values of T_r and low noise contamination have observed modulation indices no larger than about 0.3.

As noted in the Introduction, longer term (and lower frequency) studies of pulsar fluxes have reported long-term modulation depths near 1.0 (HFK; McAdam 1981). However, HFK tabulated a different modulation index $M_I = \langle I^2\rangle^{1/2}/\langle I\rangle$, a fact which was first pointed out to us by R. Narayan. We have tabulated $m_I \equiv \langle (I - \langle I\rangle)^2\rangle^{1/2}/\langle I\rangle$. They are related by $m_I = (M_I^2 - 1)^{1/2}$. For convenience of intercomparison we have tabulated both of these modulation indices in Table 5. Note that with this modification, their measured values of modulation index are mainly in the range $0.30 < m_I < 0.60$, which is larger than the modulation that we have found here, but not dramatically so. Their observations clearly show impulsive features of undetermined origin that may partly explain the discrepancy in the modulation indices. It is worth noting that their 390 MHz data, which should have a shorter RISS time scale, attain larger modulation indices than the lower frequency data. It may be that RISS fluctuations have considerable power at time scales much longer that T_r, which only shows up in very extended observations.

McAdam's data on the Vela pulsar (PSR 0833−45) is sug-

TABLE 4

REFRACTIVE SCINTILLATION TIME SERIES

PSR	ν (MHz)	T_r (days)	$T_{r\,(\mathrm{obs})}$ (days)	$D_{n,\mathrm{pred}}$ (log)	$D_{n,\mathrm{obs}}$ (log)	b
0329+54.....	310	28	>16	−1.06	−1.69	1.4
0329+54.....	416	15	>16	−0.75	−1.86	0.9
0329+54.....	750	4	2	−0.13	−1.29	0.1
0355+54.....	310	21	>16	−2.71	−1.70	0.4
0355+54.....	416	11	>16	−1.91	−1.43	1.3
1844−04.....	310	260	>16	−2.02	−1.53	0.9
1933+16.....	750	57	>16	−2.24	−2.86	1.3
2217+47.....	310	19	>16	−2.05	−2.41	1.6
2217+47.....	416	10	>16	−1.30	−1.63	1.0
2217+47.....	750	3	>2	−0.75	−1.20	0.4
2255+58.....	750	39	>16	−1.91	−1.82	0.5

TABLE 5

PREVIOUSLY PUBLISHED MODULATION INDICES[a]

PSR	M (156 MHz)	M (390 MHz)	m (156 MHz)	m (390 MHz)
0329+54.....	1.06	1.07	0.35	0.38
0823+26.....	1.10	1.13	0.46	0.53
1133+16.....	1.12	1.21	0.50	0.68
1508+55.....	1.08	1.18	0.41	0.63
1919+21.....	1.12	1.11	0.50	0.48
2217+47.....	1.08	1.42	0.41	1.01

[a] From Helfand, Kuhlman, and Fowler 1977.

gestive of a large modulation depth, although an exact value is hard to determine because the flux measurements are sparsely sampled. The most continuous monitoring session, from 1975.2 to 1976.2, shows flux variation of a factor of 2 over what appears to be a significant portion of a fluctuation time scale. This is roughly consistent with the moderate modulation depths we have observed.

d) Refractive Scintillation: Spectral Slope

We turn next to the power-law index in the structure regime of the RISS structure function plots. Note that many of the structure functions in Figures 9–12 have power-law behavior over many octaves of time lag (e.g., PSR 0329+54 at 310 MHz and 416 MHz and PSR 1933+16 at 750 MHz). This is to be expected if the length of the observing span is shorter than the longest time scales in the RISS modulation. Discussions with J. Goodman and R. Romani have alerted us to the importance of this behavior. Long stretches of power-law behavior in the structure function indicate that the random process under study is far from saturation. Using the formalism developed in Romani, Narayan, and Blandford (1986) and Goodman and Narayan (1985), Goodman has shown that $D(\tau) \propto \tau^{\alpha-3}$ for an extended medium in this regime (private communication). Here α is the exponent of the three-dimensional inhomogeneity power spectrum, $\Phi_k \propto k^{-\alpha}$, where k is the spatial wavenumber. R. Romani (private communication) has established the same result numerically.

A measurement of the power-law slope of the structure function for lags much less than the saturation time scale would seem to contain valuable information about the density inhomogeneity spectrum of the interstellar medium since $\alpha = 3 + b$. If we could be sure that the interstellar medium was essentially continuous, this would indeed be the case. As has been pointed out to us by the referee, however, the situation changes dramatically for a thin-screen geometry (also see Hjellming and Narayan 1986). Then $b = 2$ and b contains no information about the steepness of the inhomogeneity spectrum. Furthermore, as has been demonstrated by Coles (1988), it takes only a small gap in the medium in the vicinity of the observer to move from the extended medium to the thin-screen regime. Thus, unless the interstellar medium is highly uniform, a condition that is not supported by other observations or expected theoretically, results on the slope of the intensity structure function far from saturation will not be informative.

We have estimated the power-law slope for the 11 time series in Figures 9–12. The presence of noise in the time series complicates the analysis since it tends to flatten the power-law slope of the structure function, underestimating b and α. We tabulate the predicted and observed values of noise in the structure functions in Table 4. In this table we also present an estimate of b determined by fitting a line through the power-law regime of each structure function once the noise bias has been removed. These fits include the value of the structure funtion at 32 day lag, which is not plotted in Figures 9–12. The estimate of $D_{\rm noise}$ was generally $D_{\rm noise} = D(1)$, except in those cases for which $D(1)$ was not the smallest value of the structure function. In these cases a value of $D_{\rm noise}$ was found by extrapolation from the first few lags of the structure function. The uncertainty in these b values is typically ± 0.2. The mean of these b values is 0.9, although there is considerable spread in both directions. The best RISS data in our study, those for PSR 2217+47, are particularly intriguing since they show two clearly differen slopes for the structure functions at 416 and 750 MHz. We have also used the structure function behavior to estimate a characteristic time scale for the time series in a few cases. These estimates (and lower limits) are consistent with fluctuations caused entirely by RISS.

IV. SUMMARY

We have clarified a number of points about RISS with these observations. First, we have shown that there is good reason to believe that pulsars are intrinsically stable continuum sources—at least on time scales between 5 minutes and 40 days. Hence they are valuable sources to use for further studies of RISS.

We have shown that the modulation index of RISS m_r is not large (≥ 1). It typically has a value between 0.2 and 0.3 in pulsars whose RISS time scale is about half the time span of our observations. For pulsar-frequency combinations such that the predicted RISS time scale is long compared to 40 days, m_r is consistently lower than for those for which $T_r \leq 40$ days. This is to be expected if T_r correctly predicts the true RISS time scale, since the modulation index of these time series should be damped by $\approx$(40 days/T_r). There is no obvious frequency dependence of m_r, although the exponent of the dependence would have to be steeper than about 1.5 in order to produce an observable effect. Over the shorter time span of our observations we do not see the larger modulation reported by HFK and later seen in flux monitoring of the Vela pulsar over a 12 yr period (McAdam 1981). This is explicable if either the time scale for RISS variation is much larger than predicted by RISS theory or if the RISS fluctuations have a large amount of power in very low-frequency spectral components. This would give rise to a larger modulation index as the averaging time is increased.

Our data also show that the predictions for the refractive scintillation time scale T_r arising from RISS theory and DISS measurements are qualitatively correct (that is, within a factor of 3 in either direction). In two cases in which we were able to estimate observed refractive time scales, they agreed within a factor of 2 with the predicted values. Further observations, over a longer observing interval and with improved suppression of DISS noise, are necessary to test these predictions more quantitatively.

Finally, since pulsars are intrinsically stable point sources, we may use their observed long-term variability to estimate the effects of RISS on extended extragalactic sources. The pulsar observations show that RISS is caused by scattering in regions with angular size $\theta \leq 10^{-3}$ arcsec at $\nu \approx 1$ GHz and that modulation indices as large as $m \approx 0.3$ result. Extragalactic sources with intrinsic angular sizes $\theta_i \approx 10^{-3}$ will therefore undergo RISS as well, with somewhat lower modulation indices. Their RISS time scales will be slower (months instead of weeks) because extragalactic sources are extended and because they have nearly zero proper motion. The expected RISS parameters for extragalactic sources are consistent with the observed variations of extragalactic sources at $\nu \leq 1$ GHz (e.g., Altschuler *et al.* 1984).

We would like to thank the staff of the NRAO 91 m telescope for their diligence and care in running this long program of observations. We would also like to thank Jim Cordes, Jeremy Goodman, Ramesh Narayan, Roger Romani, Barney Rickett, and John Simonetti for illuminating discussions about refractive scintillation.

APPENDIX

SCINTILLATION EQUATIONS

Figure 13 shows the scattering geometry for a pulsar at distance L, embedded in the interstellar medium. The scattering medium actually filling the line of sight has been approximated by a thin screen midway between the point source and the observer. Radiation is scattered through an angle $2\theta \ll 1$ rad by electron-density fluctuations with a range of sizes a crossing the line of sight with transverse velocity $v_\perp$.

Diffractive scintillations (DISS) are rapid intensity variations produced by the *smallest* electron-density fluctuations (diameter a_d) capable of introducing phase differences $\Delta\phi \geq \pi$ rad between adjacent ray paths (see Scheuer 1968). The geometric phase delay along the bent ray path shown in Figure 13 is $\phi = \pi L\theta^2 \nu/c$, where ν is the radiation frequency. The adjacent ray with *average* path separation a along the line of sight is displaced by $2a$ at the screen, and the phase difference between these two rays is $\Delta\phi \approx \pi\nu[(L\theta + 4a)^2 - (L\theta)^2]/(cL) \approx 8\pi\theta a\nu/c$. The value a_d for which $\Delta\phi = \pi$ is $a_d \approx c/(8\theta\nu)$. The DISS time scale T_d (usually defined as the half-width to the e^{-1} point of the intensity autocovariance function) is $T_d \approx 3a_d/(5v_\perp)$ since the e^{-1} radius of a Gaussian is nearly equal to $\frac{3}{5}$ the half-intensity diameter. Thus

$$T_d \approx 3c/(40\theta\nu v_\perp) . \tag{A1}$$

Diffractive scintillations decorrelate over a bandwidth $\Delta\nu_d$ (normally taken to be the half-width to half-maximum of the autocovariance function). From the uncertainty principle, $\Delta\nu_d \approx (2\pi T_g)^{-1}$, where $T_g \approx L\theta^2/(2c) \approx \phi/(2\pi\nu)$ is the geometric time delay, so

$$\Delta\nu_d \approx c/(\pi L\theta^2) . \tag{A2}$$

Refractive scintillations (RISS) are slow intensity fluctuations produced by the *largest* electron-density fluctuations (diameter a_r) that fit in the ray bundle. This scale is approximately equal to the *average* path separation along the line of sight, or $a_r \approx L\theta/2$ (Rickett, Coles, and Bourgois 1984). The e^{-1} time scale T_r of refractive scintillations is then

$$T_r \approx 3L\theta/(10v_\perp) . \tag{A3}$$

Equations (A1) and (A2) can be used to eliminate the unknowns L, θ, and $v_\perp$ in favor of the DISS observables T_d and $\Delta\nu_d$:

$$T_r \approx \frac{4}{\pi}\left(\frac{\nu T_d}{\Delta\nu_d}\right) . \tag{A4}$$

Equation (A4) gives the pulsar RISS time scale T_r only for the frequency ν at which both its DISS time scale T_d and decorrelation bandwidth $\Delta\nu_d$ have been measured.

Values of T_r observed at different frequencies may be found from scaling laws that depend on the spectrum of electron-density fluctuation sizes a. When a ray of frequency ν passes through a single electron-density fluctuation of rms amplitude $(\Delta n^2)^{1/2}$, it bends through an angle $\Delta\theta \propto \nu^{-2}(\Delta n^2)^{1/2}$. The number of electron-density fluctuations encountered along the line of sight is proportional to L/a, so the total scattering angle $2\theta \propto \nu^{-2}(\Delta n^2)^{1/2}(L/a)^{1/2}$ (see Scheuer 1968). If there is a power-law spectrum of fluctuation sizes: $\Phi(k) = C_N^2 k^{-\alpha}$, where $k \equiv (2\pi/a)$ in three dimensions, then $\Delta n^2 \propto C_N^2 a^{\alpha-3}$. Inhomogeneities with the smallest sizes a produce the largest scattering angles θ if $\alpha < 4$, and the largest a dominate for $\alpha > 4$, so the observed scattering angle obeys

$$\theta \propto \nu^{-2} L^{1/2} (C_N^2)^{1/2} a_*^{(\alpha-4)/2} , \tag{A5}$$

where $a_* = a_d$ if $\alpha < 4$ and $a_* = a_r$ if $\alpha > 4$.

For $\alpha < 4$ and a given pulsar (fixed C_N^2, $v_\perp$, and L), $\theta \propto \nu^{\alpha/(2-\alpha)}$ and equation (A1) implies

$$T_d \propto \nu^{2/(\alpha-2)} \qquad (\alpha < 4) . \tag{A6}$$

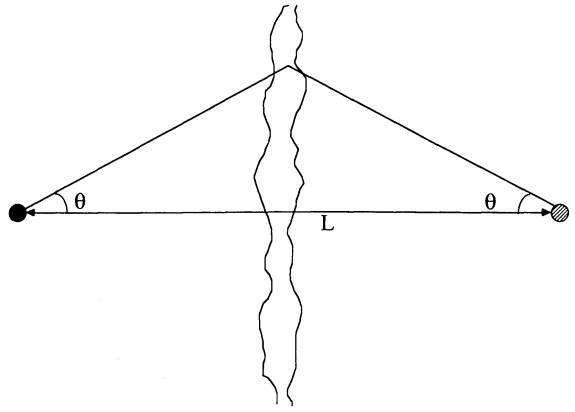

FIG. 13.—Scattering geometry for a galactic pulsar with scattering occurring in a thin screen along the line of sight

Similarly equations (A2) and (A5) combine to give the scaling law

$$\Delta\nu_d \propto \nu^{2\alpha/(\alpha-2)} \qquad (\alpha < 4)\,, \tag{A7}$$

and equations (A4) and (A5) result in

$$T_r \propto \nu^{\alpha/(2-\alpha)} \qquad (\alpha < 4)\,. \tag{A8}$$

Similarly as for equations (A6)–(A8), the corresponding scaling laws for $\alpha > 4$ are $\theta \propto \nu^{4/(\alpha-6)}$ and

$$T_d \propto \nu^{(\alpha-2)/(6-\alpha)} \qquad (\alpha > 4)\,, \tag{A9}$$

$$\Delta\nu_d \propto \nu^{8/(6-\alpha)} \qquad (\alpha > 4)\,, \tag{A10}$$

$$T_r \propto \nu^{4/(\alpha-6)} \qquad (\alpha > 4)\,. \tag{A11}$$

Thus a pulsar with DISS parameters $T_d(\nu_0)$ and $\Delta\nu_d(\nu_0)$ measured at one frequency ν_0 will have an RISS time scale $T_r(\nu)$ at any frequency ν given by either

$$T_r(\nu) = \frac{4}{\pi}\left[\frac{\nu_0\, T_d(\nu_0)}{\Delta\nu_d(\nu_0)}\right]\left(\frac{\nu}{\nu_0}\right)^{\alpha/(2-\alpha)} \qquad (\alpha < 4) \tag{A12a}$$

or

$$T_r(\nu) = \frac{4}{\pi}\left[\frac{\nu_0\, T_d(\nu_0)}{\Delta\nu_d(\nu_0)}\right]\left(\frac{\nu}{\nu_0}\right)^{4/(6-\alpha)} \qquad (\alpha > 4)\,. \tag{A12b}$$

The values in Table 1 were calculated for the particular case $\alpha = 11/3$ (Kolmogorov spectrum), but T_r varies only slowly with α for $\alpha \approx 4$.

REFERENCES

Altschuler, D. R., Broderick, J. J., Condon, J. J., Dennison, B., Mitchell, K. J., O'Dell, S. L., and Payne, H. E. 1984, *A.J.*, **89**, 1784.
Blandford, R., and Narayan, R. 1985, *M.N.R.A.S.*, **213**, 591.
Blandford, R., Narayan, R., and Romani, R. W. 1986, *Ap. J.* (*Letters*), **301**, L53.
Broderick, J. J., and Condon, J. J. 1975, *Ap. J.*, **202**, 596.
Cawthorne, T. V., and Rickett, B. J. 1985, *Nature*, **315**, 40.
Cole, T. W., Hesse, H. K., and Page, C. G. 1970, *Nature*, **225**, 712.
Coles, W. A. 1988, in *Radio Wave Scattering in the Interstellar Medium*, ed. J. M. Cordes, B. J. Rickett, and D. C. Backer (New York: AIP), p. 163.
Cordes, J. M. 1986, *Ap. J.*, **311**, 183.
Cordes, J. M., Pidwerbetsky, A., and Lovelace, R. V. E. 1986, *Ap. J.*, **310**, 737.
Cordes, J. M., Rickett, B. J., and Backer, D. C., eds. 1988, *Radio Wave Scattering in the Interstellar Medium* (AIP Conference Proceedings 174) (New York: AIP).
Cordes, J. M., Weisberg, J. M., and Boriakoff, V. 1985, *Ap. J.*, **288**, 221.
Cordes, J. M., and Wolszczan, A. 1986, *Ap. J.* (*Letters*), **307**, L27.
Dennison, B., and Condon, J. J. 1981, *Ap. J.*, **246**, 91.
Fiedler, R. L., Dennison, B. K., Johnston, K. J., and Hewish, A. 1987, *Nature*, **326**, 675.
Goodman, J., and Narayan, R. 1985, *M.N.R.A.S.*, **214**, 519.
Heeschen, D. S. 1984, *A.J.*, **89**, 1111.
Helfand, D. J., Fowler, L. A., and Kuhlman, J. V. 1977, *A.J.*, **82**, 701 (HFK).
Hesse, K. H. 1972, *Nature*, **235**, 27.
Hewish, A., Wolszczan, A., and Graham, D. 1985, *M.N.R.A.S.*, **213**, 167.
Hjellming, R. M., and Narayan, R. 1986, *Ap. J.*, **310**, 768.
McAdam, W. B. 1981, *Proc. Astr. Soc. Australia*, **4**, 219.
Rickett, B. J. 1986, *Ap. J.*, **307**, 564.
Rickett, B. J., Coles, W. A., and Bourgois, G. 1984, *Astr. Ap.*, **134**, 390.
Romani, R. W., Blandford, R. D., and Cordes, J. M. 1987, *Nature*, **328**, 324.
Romani, R. W., Narayan, R., and Blandford, R. 1986, *M.N.R.A.S.*, **220**, 19.
Scheuer, P. A. G. 1968, *Nature*, **218**, 920.
Sieber, W. 1982, *Astr. Ap.*, **113**, 311.
Simonetti, J. H., Cordes, J. M., and Heeschen, D. S. 1985, *Ap. J.*, **296**, 46.
Taylor, A. R., and Gregory, P. C. 1983, *A.J.*, **88**, 1784.
Weisberg, J. M., Armstrong, B. K., Backus, P. R., Cordes, J. M., Boriakoff, V., and Ferguson, D. 1986, *A.J.*, **92**, 621.

J. J. CONDON: National Radio Astronomy Observatory, Edgemont Road, Charlottesville, VA 22901

D. R. STINEBRING: Physics Department, P.O. Box 708, Princeton University, Princeton, NJ 08544